

 Open access • Journal Article • DOI:10.1016/J.JNNFM.2010.09.007

## The slow retraction method (SRM) for the determination of ultra-short relaxation times in capillary breakup extensional rheometry experiments — [Source link](#)

[Laura Campo-Deaño](#), [Christian Clasen](#)

**Institutions:** [Katholieke Universiteit Leuven](#)

**Published on:** 01 Dec 2010 - [Journal of Non-newtonian Fluid Mechanics](#) (Elsevier)

**Topics:** [Viscous liquid](#), [Breakup](#), [Capillary action](#) and [Newtonian fluid](#)

Related papers:

- [Elasto-capillary thinning and breakup of model elastic liquids](#)
- [Effect of a spectrum of relaxation times on the capillary thinning of a filament of elastic liquid](#)
- [How dilute are dilute solutions in extensional flows](#)
- [Capillary break-up rheometry of low-viscosity elastic fluids](#)
- [How to extract the Newtonian viscosity from capillary breakup measurements in a filament rheometer](#)

Share this paper:    

View more about this paper here: <https://typeset.io/papers/the-slow-retraction-method-srm-for-the-determination-of-4r25na41yv>

# The slow retraction method (SRM) for the determination of ultra-short relaxation times in capillary break-up extensional rheometry experiments

Laura Campo-Deaño, Christian Clasen\*

*Department of Chemical Engineering, Katholieke Universiteit Leuven, Willem de Croylaan 46, 3001 Heverlee, Belgium*

---

## Abstract

We monitor the capillary thinning and breakup of low viscous liquid filaments with high speed imaging to determine the relaxation time of dilute polymer solutions in extension. The induction of filament thinning by a slow extension of a liquid bridge beyond the static stability limit enables one to create axially symmetric thinning profiles with minimized inertial oscillations from acceleration of the liquid. The minimized disturbance of the capillary thinning process by this slow retraction method (SRM) allows the observation and quantitative fitting of the visco-capillary and inertio-visco-capillary balance as well as the potential flow regime for a series of Newtonian liquids covering a viscosity range from 350 to 27 mPa s. For dilute solutions of polyethylene oxide in water the SRM allows the reliable determination of relaxation times in extension of as low as 240  $\mu$ s. A lower limit for the polymer concentration  $c_{low}$  below which an elasto-capillary balance cannot be observed is introduced, based on the finite extensibility limit  $L^2$  of the

---

\*Corresponding author. Tel: +32 16 3 22354; Fax: +32 16 3 22991  
*Email address:* christian.clasen@cit.kuleuven.be (Christian Clasen)

polymer chain.

*Keywords:* Capillary thinning, Caber, extensional rheometer, static stability limit, elongational rheometry, dilute polymer solution, relaxation time, elasto-capillary balance, self-similarity, finite extensibility, critical concentration.

---

## 1. Introduction

2     The uniaxial extensional viscosity  $\eta_E$  is a fundamental material prop-  
3     erty of a fluid which characterizes the resistance of a material to an uniaxial  
4     stretching deformations. While for rheologically simple fluids this viscosity  
5     is directly related to the shear viscosity  $\eta$  via the Trouton ratio  $\eta_E = 3\eta$ ,  
6     for complex (micro-structured) or viscoelastic fluids, this extensional viscos-  
7     ity can be a function of both the rate of deformation and the total strain  
8     accumulated. In particular the highly increased extensional viscosity of vis-  
9     coelastic solutions in comparison to simple fluids of similar shear viscosity  
10    has a strong impact on operations as mixing, pumping, spraying, coating and  
11    general processing or transport operations. The strong increase of viscoelastic  
12    material functions in extensional flows has a particularly pronounced effect  
13    in dilute polymer solutions due to the unraveling and extension of the ini-  
14    tially coiled polymeric molecules by the strong extensional flows, whereas a  
15    contribution of the polymer to the shear viscosity is negligible [1, 2, 3, 4, 5].  
16    One flow type where the effects of dissolved polymers on the extensional flow  
17    becomes especially apparent is the thinning and breaking of liquid filaments,  
18    since this free-surface flow is readily observable. Already the pioneering work  
19    of Middleman [6] and Goldin et al. [7] have shown the dramatic effects of

20 minute amounts of high-molecular-weight additives on the breakup of fluid  
21 filaments. For the case of jets of dilute polymer solutions the elastic stresses  
22 generated affect the breakup length of the jet and the ensuing droplet size  
23 distribution [8, 9]. For a low viscous, dilute polymer solution dripping from  
24 a faucet, the presence of the polymer can dramatically extend the time to  
25 pinch off and inhibit the existence of satellite droplets [10, 4, 11].

26 A quantitative description of the effects of polymer additives on low vis-  
27 cosity dilute polymer solutions requires a precise determination of the actual  
28 material properties in an extensional flow and therefore experimental tech-  
29 niques that allow their reliable measurement at relevant deformation rates.  
30 While for higher viscosity systems techniques as the Meissner [12, 13] or  
31 Münstedt apparatus [14, 15] have been introduced already a while ago, gen-  
32 erating and measuring purely extensional flows of lower viscous, mobile fluids  
33 has proven to be extremely difficult. Attempts have been made to do this  
34 via the determination of pressure drop in porous media [16], opposed jet de-  
35 vices [17], spin-line rheometers and two- and four-roll mills [18, 19]. First  
36 reliable mechanical studies of the state of stress of lower viscous liquids in  
37 a well-defined uniaxial flow field were made by Sridhar et al. [20] using the  
38 filament stretching device, but were still limited to viscosities  $> 1 \text{ Pa s}$  [21].  
39 Only recently the capillary breakup extensional rheometry (Caber) has been  
40 introduced, that determines extensional flow material functions directly from  
41 the thinning dynamics of a liquid filament [2, 22, 23]. A capillary break-up  
42 experiment creates an unstable fluid filament by imposing a rapid axial step-  
43 strain of prescribed magnitude to a small fluid element. The formed liquid  
44 filament is then allowed to thin under the action of surface tension until it

45 finally breaks. The decay of the necking sample is governed by a balance of  
46 viscous, elastic, gravitational and capillary forces. A capillary breakup ex-  
47 periment has therefore no active control over the uniaxial deformation rate  
48 that a filament experiences and is therefore often considered to be an ‘in-  
49 dexer’ rather than an actual rheometer. However, for several special cases  
50 the Caber experiment can deliver absolute material properties, as for example  
51 an extensional viscosity for a Newtonian liquid [24], the power law index of an  
52 extension thinning fluid [25, 26], a yield stress against a uniaxial deformation  
53 [27, 28], or the longest relaxation time in an extensional flow [29]. In particu-  
54 lar the possibility to determine and compare the extensional relaxation time  
55 to the shear relaxation time has been the subject of in-depth investigations  
56 [30, 31, 32, 3, 19, 23, 33, 34, 5, 4, 35, 36]. But although the Caber technique  
57 enables one to investigate fluids with viscosities below the limiting value of  
58 the filament stretching technique of 1 Pa s, Rodd et al. [37] have shown  
59 that there is also for the Caber technique a lower viscosity limit which is for  
60 Newtonian systems at  $\sim 70$  mPa s. The main limitation from an experi-  
61 mental point of view arises from the difficulty to create a low viscous liquid  
62 filament fast enough so that the thinning dynamics can still be observed. In  
63 a general Caber experiment the liquid filament is created outgoing from a  
64 drop of the fluid confined between two parallel circular plates that are sub-  
65 sequently quickly separated to a desired separation distance. The necessary  
66 fast acceleration and deceleration of the liquid when performing this initial  
67 stretch to create a filament of a low-viscous liquid are inherently coupled  
68 with inertia induced oscillations of the end droplets adhered to the endplates  
69 and an axial asymmetric filament profile. The effect of these oscillations on

70 the thinning dynamics of the filament cannot be ignored at low viscosity levels  
71 and prevent a quantitative evaluation of the thinning dynamics below the  
72 critical limit indicated by Rodd et al. [37]. Furthermore, the inertial effects  
73 present also a limit to the determination of a relaxation time  $\lambda$  with a Caber  
74 experiment. Although the stabilizing effect of the polymer lowers the acces-  
75 sible viscosities to  $\sim 1$  mPa s, Rodd et al. [37] gave an empirical lower limit  
76 for the relaxation time determination of  $\sim 1$  ms [37]. Recently Vadillo et al.  
77 [38] presented with the Trimaster a Caber type experimental setup utilizing  
78 high speed plate separations that allowed to reliably determine the thinning  
79 dynamics of dilute polymer solutions with viscosities down to 10 mPa s and  
80 that could detect breakup time delays caused by the polymer of order 5  
81 ms. For even lower viscosities and relaxation times, detailed investigations  
82 of the breaking dynamics of liquid threads had so far to rely on simulation  
83 techniques. Recent results by Bath et al. [39] using the Oldroyd-B model,  
84 and Ardekani et al. [40] using the Giesekus model were able to model the  
85 breaking dynamics and satellite drop formation for filaments with relaxation  
86 times down to  $O(1$  ms) and viscosities of  $O(1$  mPa s). However, as correctly  
87 stated in [40], "the [experimental determination of extensional viscoelastic  
88 properties for these] very low viscosity and weakly elastic liquids ... is a  
89 particular challenge using traditional rheometers", and "filament stretching  
90 devices or Caber devices cannot be used to measure the tensile properties of  
91 such low-viscosity liquid(s) because of the rapid timescales for breakup".

92 Still, an experimental technique that could probe (aqueous) solutions  
93 with viscosities of order  $O(1$  mPa s) to determine relaxation times in uni-  
94 axial extensional free surface flows at the sub-millisecond scale is highly de-

95 sirable, since applications as for example ink-jet printing or atomization of  
96 drug loaded formulations in medical or pharmaceutical applications operate  
97 at thinning velocities where sub-millisecond relaxation times are dominant  
98 [41, 42] and where the addition of traces of polymers is used to structure the  
99 breaking dynamics and size and occurrence of satellite droplets [43].

100 In this paper we present therefore with the slow retraction method (SRM)  
101 a modified usage protocol of the general Caber setup that enables the reliable  
102 determination of breakup time delays and relaxation times of order  $O(200 \mu\text{s})$   
103 in aqueous systems with viscosities of  $O(1 \text{ mPa s})$ . The paper is structured  
104 as follows:

105 In the Materials and Methods section the operating principle of the slow  
106 retraction method to create a liquid filament of a low viscous liquid is in-  
107 troduced. The second section focuses then on the thinning behaviour of low  
108 viscous, Newtonian liquids. The third section discusses the thinning dynam-  
109 ics of dilute aqueous polymer solutions and introduces the theoretical limits  
110 of the slow retraction method for the detection of sub-millisecond relaxation  
111 times.

## 112 **2. Materials and Methods**

### 113 *2.1. Experimental Setup*

114 The capillary thinning experiments were carried out using the plate separa-  
115 tion drive unit of a Haake CaBER-1 extensional rheometer (Thermo Haake  
116 GmbH, Karlsruhe, Germany) in order to control the position and separation  
117 velocities of two circular parallel plates with selectable diameters  $D_p$  of 4, 6  
118 and 8 mm. Fluid samples were carefully loaded between the plates using a

119 syringe to ensure the absence of trapped air bubbles in the sample as well  
120 as between the sample and the plates. During and after the controlled sep-  
121 aration of the plates to a final distance the evolution of the thinning fluid  
122 filament forming between the plates was monitored with video imaging us-  
123 ing a high speed camera (Photron Fastcam SA-2, Photron, San Diego CA,  
124 USA) with a 12X zoom lens and two 2X extensions (Navitar, Rochester NY,  
125 USA), together with a fiber optic backlight source as shown in Figure 1. Each  
126 experimental test was repeated at least four times in order to corroborate  
127 reproducibility.



Figure 1: Experimental set up for the CaBER.

128 The video images were subsequently analyzed by digital image processing



129 in Matlab in order to determine the full filament profile and in particular the  
 130 position and dimension of the minimum filament diameter  $D_{min}$ . In order  
 131 to calibrate the diameters determined from the image processing, a series of  
 132 standard diameter filaments (0.02, 0.03, 0.06, 0.12, 0.25, 0.50 and 1 mm) has  
 133 been measured with the optical setup at the same experimental conditions.  
 134 The correlation between the actual and observed diameters is given in Figure  
 135 2 and used for all subsequent investigations.

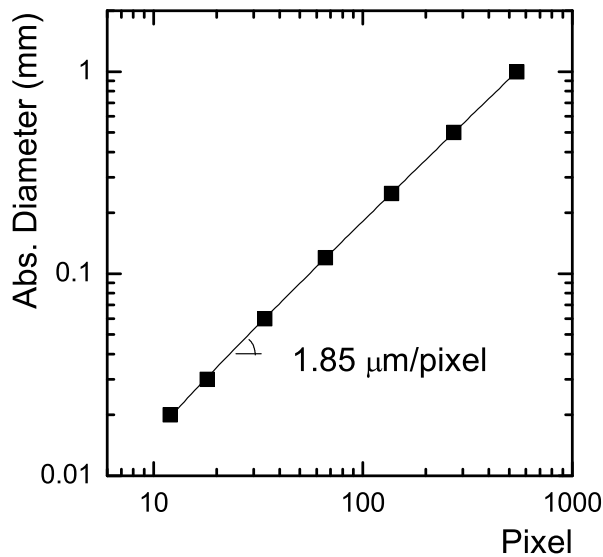


Figure 2: Millimeter to pixel ratio of the experimental setup, determined from images of fibers with absolute diameters of 0.02, 0.03, 0.06, 0.12, 0.25, 0.50 and 1 mm.

136 *2.2. The slow retraction method (SRM)*

137 For the creation of low viscous liquid filaments whose thinning dynamics  
 138 are subsequently monitored we followed a procedure that is different from the  
 139 general capillary breakup extensional rheometry (Caber) protocols. Start-

140 ing from the initial cylindrical liquid bridge with an initial aspect ratio of  
 141  $\Lambda_0 = L_0/(2R_{mid}) = L_0/D_p$  (where  $L$  generally denotes the plate separation  
 142 distance and  $R_{mid}$  the liquid bridge radius at  $L/2$ ), the plates are separated  
 143 with a moderate velocity of  $\sim 2$  mm/s just slightly below a critical aspect  
 144 ratio  $\Lambda_{S,break}$  at which a statically stable liquid bridge (indicated by the suffix  
 145 S) still exists.

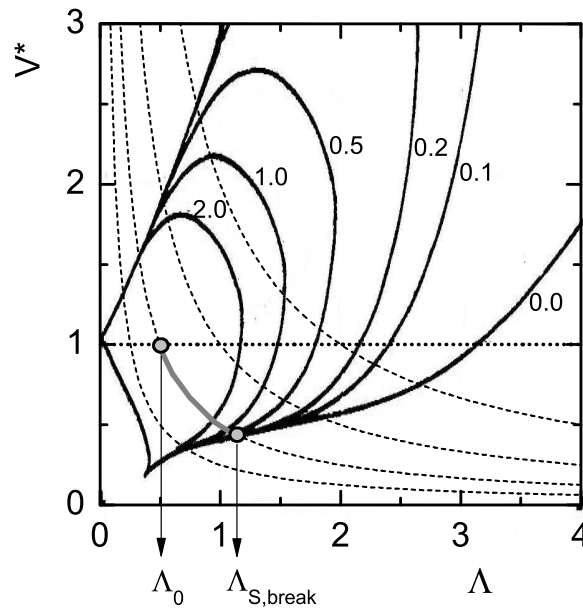


Figure 3: Critical volume stability limits  $V^*_{break}$  (solid lines, taken from [44]) as a function of the aspect ratio  $\Lambda$  for different Bond numbers  $Bo$  (indicated as numbers in the diagram). The dashed hyperbolas (eq. (1)) represent constant absolute fluid volumina. The dotted line indicates a cylindrical filament ( $V^* = 1$ ). The indicated initial aspect ratio  $\Lambda_0$  and the critical aspect ratio  $\Lambda_{S,break}$  represent the values selected for measurements in the present paper

146 The critical aspect ratio of  $\Lambda_{S,break}$  above which the liquid bridge becomes

147 unstable and collapses can be determined from the stability diagrams for  
 148 liquid bridges of Slobozhanin et al. [44]. These diagrams give critical values  
 149 of the dimensionless fluid volume

$$V^* = \frac{4V_0}{\pi D_p^2 L} \quad (1)$$

150 as a function of the aspect ratio  $\Lambda$ . Here  $V_0$  refers to the total volume of  
 151 the fluid which can be calculated from that of the initial cylindrical bridge as  
 152  $(\pi D_p^2 L_0)/4$ . The diagram in Figure 3 depicts (as solid lines) the critical vol-  
 153 ume stability limit  $V_{break}^*$  (beyond which the filament collapses) as a function  
 154 of the aspect ratio  $\Lambda$  for different Bond numbers  $B_0 = (\rho g D_p^2)/(4\gamma)$ . The  
 155 Bond number captures the effects of gravity against the surface tension and  
 156 is a measure of how much the initial cylindrical filament 'sags'. Larger plate  
 157 diameters  $D_p$  lead to more sagging and higher Bond numbers and therefore  
 158 to critical volume stability limit curves  $V_{break}^*$  that reach there collapsing limit  
 159 already at smaller critical aspect ratios  $\Lambda_{S,break}$ . Starting now for a filament  
 160 breakup experiment in this diagram from a cylindrical configuration  $V^* = 1$   
 161 (the dotted horizontal line) at  $\Lambda_0$  and holding the total physical volume con-  
 162 stant as the bridge is axially elongated by separating the plates, we follow  
 163 the hyperbolic trajectory  $V^* \sim L_0/L$  of eq. (1) (indicated as dashed lines).  
 164 The axial elongation yields statically stable filaments until the hyperbola in-  
 165 tersects the critical volume stability curve of the appropriate Bond number  
 166 and enables one to extract  $\Lambda_{S,break}$  from this intersection [27].

167 After reaching the stable separation distance just below  $\Lambda_{S,break}$ , a very  
 168 slow separation velocity of the end plates of 0.11 mm/s was chosen in order  
 169 to approach  $\Lambda_{S,break}$  and initiate the filament breaking process which then

170 subsequently evolves on a timescale orders of magnitude faster than the slow  
 171 plate separation speed . This 'slow retraction method' (SRM) assures that  
 172 the effects of fluid inertia (that were inherent for a fast plate separation as  
 173 described by Rodd et al. [37]) are minimized. Furthermore, in comparison  
 174 to a fast initial separation, the slow retraction method leads to a a fully  
 175 relaxed state of the liquid filament and its solution structure at the onset  
 176 of the filament collapse [35]. The mid-filament radius  $R_{mid}$  at this point is  
 177 denoted  $R_0$  in the following. Figure 4 compares the breaking process of a  
 178 75% solution of glycerol in water, initiated with a fast separation (upper  
 179 row) and with the slow retraction method (lower row of pictures). It can be  
 180 seen that the oscillations in the end drops are strongly reduced with the slow  
 181 retraction method and that the filament retains its axial symmetry to the  
 182 final breaking point in comparison to the fast separation.

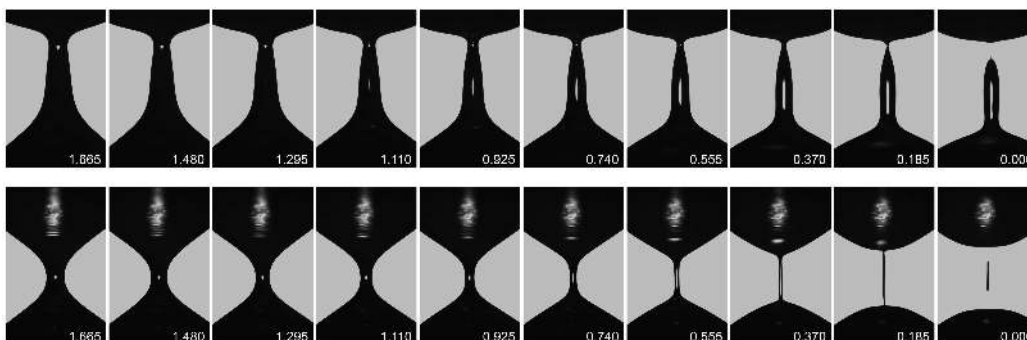


Figure 4: Comparison of the breaking dynamics induced by the slow retraction method (SRM) (bottom row) and by a fast separation (upper row) for a 75% glycerol/water mixture. The plate separation velocity of the SRM is 0.11 mm/s, and 170 mm/s for the fast separation method. The time to breakup is indicated in milliseconds on each consecutive picture. The plate diameter is  $D_p = 4$  mm ( $Bo = 0.648$ ).

183 In order to adjust the radius  $R_0$  as well as the length of the collapsing  
 184 filament, both the plate diameter  $D_p$  as well as the initial aspect ratio  $\Lambda_0$   
 185 can be varied in order to affect the critical aspect ratio  $\Lambda_{S,break}$  at which  
 186 the filament will start to thin. We still follow the same hyperbolic trajec-  
 187 tory in the stability diagram when keeping  $\Lambda_0$  constant and increasing  $D_p$ .  
 188 However, increasing  $D_p$  will lead to higher Bond numbers and therefore de-  
 189 creasing critical values  $\Lambda_{S,break}$ , but at same time increasing filament radii  
 190  $R_0$ . On the other hand, increasing the initial aspect ratio at constant plate  
 191 diameter moves the hyperbola in Figure 3 away from the origin and therefore  
 192 the intersect  $\Lambda_{S,break}$  to larger aspect ratios. Both adjustments (increasing  
 193  $D_p$  at constant  $\Lambda_0$ , and increasing  $\Lambda_0$  at constant  $D_p$ ) will lead to longer  
 194 thinning filaments at comparable radii, an effect that becomes important in  
 195 the curvature discussion below. It should be noted that also Sattler et al.  
 196 [11] have deliberately used  $\Lambda_{S,break}$  as the final aspect ratio, however, with a  
 197 fast initial separation to reach this limit.

### 198 2.3. Fluids

199 The Newtonian liquids used were aqueous solutions of glycerol (Acros  
 200 Organics, Geel, Belgium) at different concentrations of 75, 85, 90 and 95  
 201 wt%. The shear viscosity was measured using a stress-controlled rheometer  
 202 (AR-G2, TA Instruments) at  $25^\circ C$ , and the surface tension  $\gamma$  was determined  
 203 with a Wilhelmy plate method. The resulting values are shown in Table 1. As  
 204 a non-Newtonian fluid, aqueous solutions of poly(ethylene oxide) (POLYOX  
 205 Resin WSRN N-12K, Union Carbide) with a nominal mass average molecular  
 206 weight of 1.000.000 g/mol and an equilibrium surface tension of  $\gamma = 62$  mN/m  
 207 [4] were used. Solutions in pure distilled water of 0.0005, 0.001, 0.002, 0.005,

208 0.01, 0.02 and 0.05 wt% of PEO were prepared at room temperature, and  
209 gently stirred for 24 h to speed dissolution.

Table 1: Shear viscosity  $\eta$  and surface tension  $\gamma$  for the glycerol in water solutions at 25°C.

	$\eta$ (mPa s)	$\gamma$ (mN/m)
75%	$27.0 \pm 0.1$	$64.8 \pm 1$
85%	$76.8 \pm 0.1$	$64.0 \pm 1$
90%	$149.9 \pm 0.1$	$63.6 \pm 1$
95%	$319.2 \pm 0.1$	$63.0 \pm 1$

### 210 3. Results and Discussion

#### 211 3.1. Newtonian Fluids

212 Before the next chapter focuses on the filament thinning behaviour of  
213 dilute polymer solutions and the determination of relaxation times from these  
214 experiments, it is necessary to first investigate the thinning dynamics of the  
215 pure (Newtonian) solvents to validate the slow retraction method (SRM) and  
216 to determine the general effects that the SRM has on the breaking dynamics.

217 Figure 5 shows the last 4 milliseconds of filament thinning of the four  
218 glycerol solutions that span a range of viscosities from 27 to 320 mPa s at  
219 a surface tension of  $\sim 64$  mN/m (exact values in table 1). Each fluid was  
220 probed with 3 different plate diameters and 2 initial aspect ratios  $\Lambda_0$ . In  
221 order to follow the fast evolution of the filament diameter, a frame rate of  
222 5400 frames per second was selected with a resolution of 256 x 832 pixels  
223 at 1.8 microns/pixel for the video imaging. In addition to the diameter

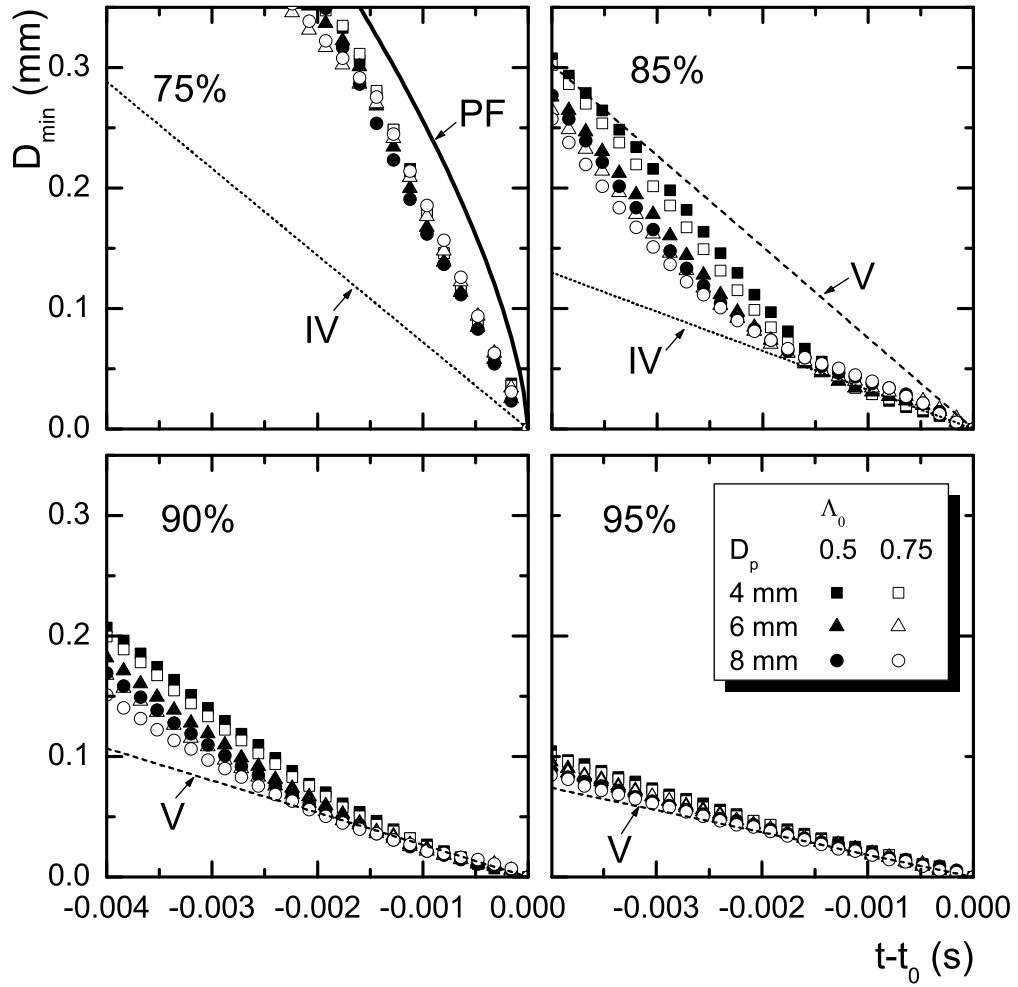


Figure 5: Time evolution of the minimum filament diameter  $D_{min}$  close to breakup for four concentrations of glycerol in water and for three different endplate diameters  $D_p$  and two initial aspect ratios  $\Lambda_0$  as indicated in the legend, at  $25^\circ C$ . Also shown are the calculated thinning curves for the visco-capillary balance (V-regime) of eq. (2) (dashed line), for the inertio-visco-capillary balance (IV-regime) of eq. (4) (dotted line), and for the PF regime of eq. (5) (solid line), using the the viscosity and surface tension of Table 1

224 evolution of Figure 5, Figure 6 gives for a plate diameter of  $D_p = 4$  mm and  
 225 an aspect ratio of  $\Lambda_0 = 0.5$  for each concentration a series of images of the  
 226 full filament shape with time intervals that directly relate to the data point  
 227 spacing in Figure 5.

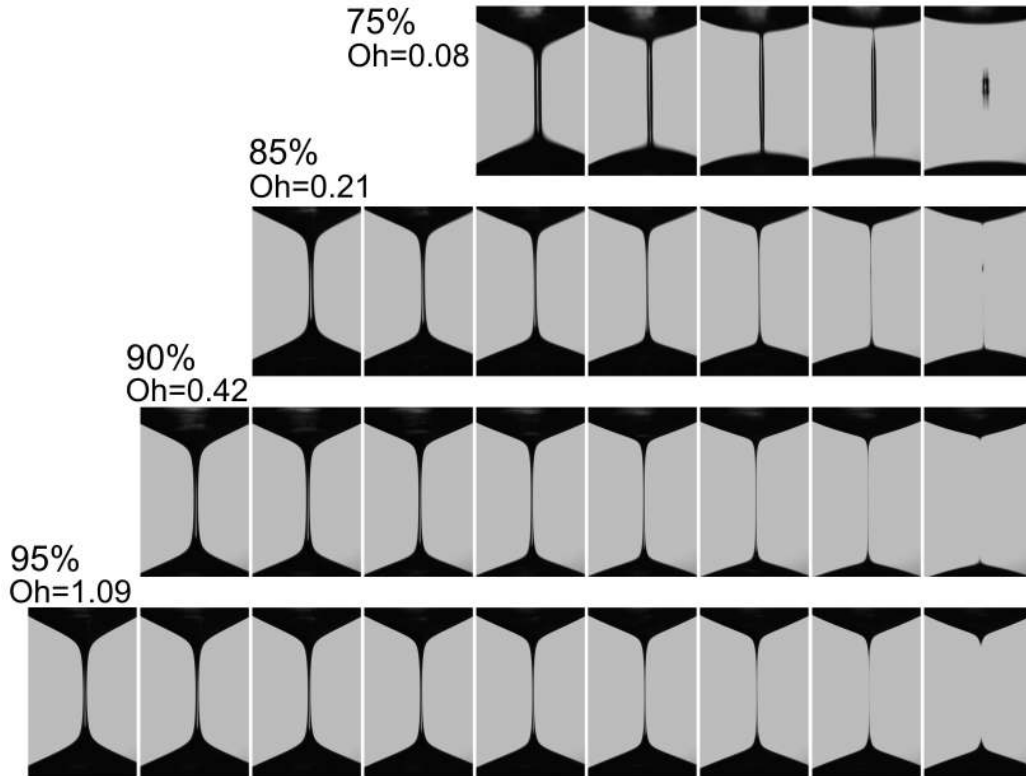


Figure 6: Thinning and pinch-off of the filament for solution of a) 75%, b) 85%, c) 90% and d) 95% of glycerol in water at  $25^\circ C$ . The time interval between each consecutive picture amounts to 0.185 ms, the plate diameter  $D_p$  used was 4 mm with an initial height of 2 mm (initial aspect ratio  $\Lambda_0 = 0.5$ ).

228 The thinning diagrams in Figure 5 represent four critical cases of the  
 229 SRM when approaching the breaking behaviour of low viscosity fluids. For



230 the highest viscous solution in Figure 5 (95 wt% glycerol) the liquid filament  
 231 decays linear with time prior to breakup and (as can be seen in Fig. 6) with  
 232 a stationary minimum filament diameter and breaking point in the middle  
 233 of the filament. This is expected, since for a sufficiently high viscosity the  
 234 squeezing action of the capillary pressure is solely balanced by the viscous  
 235 stresses in the filament. In this viscosity controlled thinning regime (in the  
 236 following indicated as 'V' regime) the slender filament that develops close  
 237 to breakup becomes independent of initial conditions and evolves in a self-  
 238 similar way with the smallest diameter  $D_{min}$  and final breaking point in the  
 239 middle of the filament. The minimum radius evolution can in this case be  
 240 described by similarity solutions [45] of which the most stable one was found  
 241 by Papageorgiou [46, 47]:

$$R_{min} = 0.0709 \frac{\gamma}{\mu} (t_0 - t), \quad (2)$$

242 where  $t_0$  is the time at filament breakup. The dashed line in Figure 5 for  
 243 the concentration 95% gives the Papageorgiou solution of eq. (2), using the  
 244 shear viscosity  $\eta$  and surface tension  $\gamma$  of Table 1.

245 For the solution of 90% Figure 5 shows that the final stages of thinning  
 246 are still in the V regime and are well described by the indicated Papageor-  
 247 giou solution (dashed line). However, the linear thinning regime is reached at  
 248 later stages as compared to the 95% solution and we can clearly observe an  
 249 accelerating thinning regime before the linear, viscosity controlled thinning  
 250 sets in. The reason for this is that the Papageorgiou solution is only appli-  
 251 cable for long, slender filaments with axial length scales much larger than  
 252 radial. On the other hand, the slow retraction method as a tool to create

253 observable filaments is deliberately using the smallest possible final aspect  
 254 ratio  $\Lambda_{S,break}$  and therefore creating the shortest possible filaments with an  
 255 inherently high axial curvature. The mean curvature  $\kappa$  of the filament surface  
 256 can be described via [48]

$$\kappa = \frac{1}{R(1+(R')^2)^{0.5}} - \frac{R''}{(1+(R')^2)^{1.5}}, \quad (3)$$

257 where  $R = R(z)$  is the radius of the filament along the axial or  $z$ -direction  
 258 and  $R' = dR/dz$  and  $R'' = d^2R/dz^2$  are the respective first and second spatial  
 259 derivatives. At the location of the minimum radius  $R_{min}$  the first derivative  
 260 is  $R' = 0$  and the second derivative reduces to the inverse of the radius  $R_z$   
 261 of the tangentially adjacent circle (indicated in Fig. 7),  $R'' = 1/R_z$ , so that  
 262 the mean curvature of eq. (3) reduces at this point to  $\kappa = 1/R_{min} - 1/R_z$ .  
 263 The apparent acceleration of the filament thinning originates then from the  
 264 initially high value of  $1/R_z$  that causes a lower mean curvature and therefore  
 265 a lower Laplace pressure at the necking point in comparison to a slender  
 266 filament of same radius  $R_{min}$ . During the thinning process  $1/R_z$  becomes  
 267 smaller, resulting in the apparent acceleration of the thinning until the mean  
 268 curvature  $\kappa = 1/R_{min} - 1/R_z$  approaches the radial curvature  $1/R_{min}$  and  
 269 the slender filament shape required for the applicability of the Papageorgiou  
 270 solution is reached.

271 Comparing the ratio of mean curvature  $\kappa$  and radial curvature  $1/R_{min}$   
 272 (shown in Figure 8 as the relative curvature  $\kappa R_{min}$ ) for representative thin-  
 273 ning experiments of 95%, 90% and 85% glycerol solutions with the observable  
 274 linear thinning range in Figure 5 enables one to determine a critical relative  
 275 curvature, below which a slender filament is reached. This critical relative  
 276 curvature is indicated in Figure 8 by the dotted line and equates to  $\kappa R_{min}$

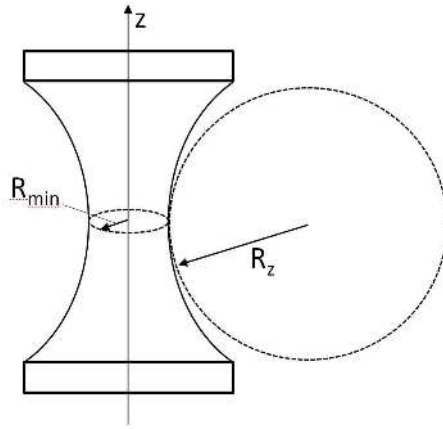


Figure 7: Schematic drawing of the filament radius  $R$  and the axial radius  $R_z$ .

277 = 1.006. This limit gives now a practical value to the general 'slenderness'  
 278 requirement for the application of similarity solution and the range of radii  
 279 where linear fits of  $R_{min} \sim (t_0 - t)$  can be used to extract material properties  
 280 from capillary thinning experiments.

281 The thinning curves of Figure 5 for 90% and 85% indicate that also the  
 282 initial aspect ratio and plate diameter have an influence on when the critical  
 283 relative curvature and a slender filament is reached when using the slow  
 284 retraction method. As it can be seen in Figure 5, increasing the end-plate  
 285 diameter from 4 to 8 mm at a constant initial aspect ratios  $\Lambda_0$  shifts the  
 286 onset of a clearly visible self similar thinning regime to earlier times. Also an  
 287 increase of the initial aspect ratio at a constant plate diameter has the same  
 288 effect. This is not unexpected as both cases increase the filament length and  
 289 decrease therefore the axial curvature at comparable radii as discussed for  
 290 the critical volume stability limit above.

291 However, both larger plate diameters and initial filling height lead to

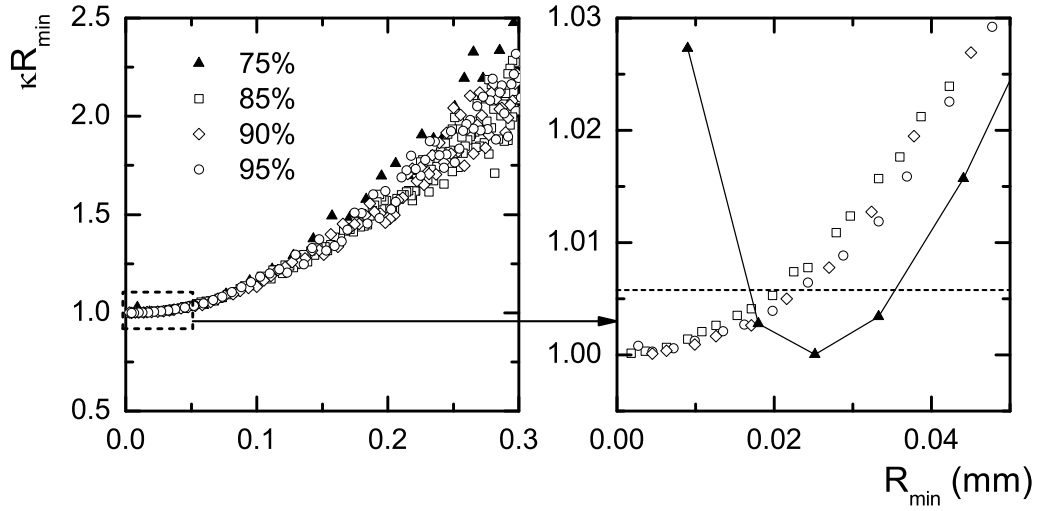


Figure 8: Ratio of the mean curvature  $\kappa$  to the radial curvature  $1/R_{\min}$  as a function of the minimum radius  $R_{\min}$ . Data for  $R_z$  were obtained from tangential fits to the digitized filament profiles of Fig. 9 at the minimum of the radius  $R(z)$ . The dotted line marks the critical relative curvature  $\kappa R_{\min}$  below which the experimental data in Figure 5 follow the linear similarity solutions.

292 larger Bond numbers and therefore less reproducible results due to difficulties  
 293 in achieving similar initial fillings of the gap. Optimal plate diameter and  
 294 initial aspect ratio for a sufficient reproducibility of the data for the current  
 295 investigation of low viscous solutions were  $D_p = 4$  mm and  $\Lambda_0 = 0.5$  which  
 296 will be used throughout the following experiments and discussions.

297 The solution of 85% glycerol in Figure 5 marks then a transition in the  
 298 thinning behaviour. While it is still possible to observe a linear thinning close  
 299 to breakup, the images of Figure 6 reveal that the filament is not breaking in  
 300 the middle anymore, but that the location of the minimum filament diameter  
 301  $D_{\min}$  is shifting in axial direction towards the end drops. This becomes more

302 obvious in Figure 9 that depicts the digitized filament profiles of figure 6  
 303 with intervals of time of 0.185 ms (The location of the minimum radius  $R_{min}$   
 304 is for each profile indicated by the bold arrows where it deviates from the  
 305 midfilament location  $z = 0$ ).

306 In this case velocities in the filament become so large that inertia can no  
 307 longer be neglected and the thinning behaviour prior to breakup is controlled  
 308 by an inertio-visco-capillary balance (the so-called 'IV' regime). The similar-  
 309 ity solution found by Eggers [49] that describes this IV thinning regime does  
 310 not contain the fluid density and differs from the visco-capillary thinning (eq.  
 311 2) only by the front factor

$$R_{min} = 0.0304 \frac{\gamma}{\mu} (t_0 - t). \quad (4)$$

312 However, the determination of the minimum filament radius requires in  
 313 this case the evaluation of the full filament shape as the location of the  
 314 minimum radius shifts away from the filament middle. A comparison of the  
 315 thinning data of the 85% solution in Fig. 5 with the IV solution of eq. (4)  
 316 (dotted line) shows good agreement.

317 For the 75% glycerol solution the shifting of the minimum filament diam-  
 318 eter  $R_{min}$  away from the middle of the filament and the final breaking close  
 319 to the enddrops becomes even more obvious in the pictures of Figure 6 as  
 320 well as in the digitized profiles of Figure 9. However, fitting the minimum  
 321 diameter data in Figure 5 with the IV solution of eq. (4) (dotted line) does  
 322 not work anymore. The thinning data for the 75% solution is much closer  
 323 to a purely inertia controlled thinning, indicated by the solid line in Figure  
 324 5. This thinning behaviour (the so called potential flow 'PF' regime), that

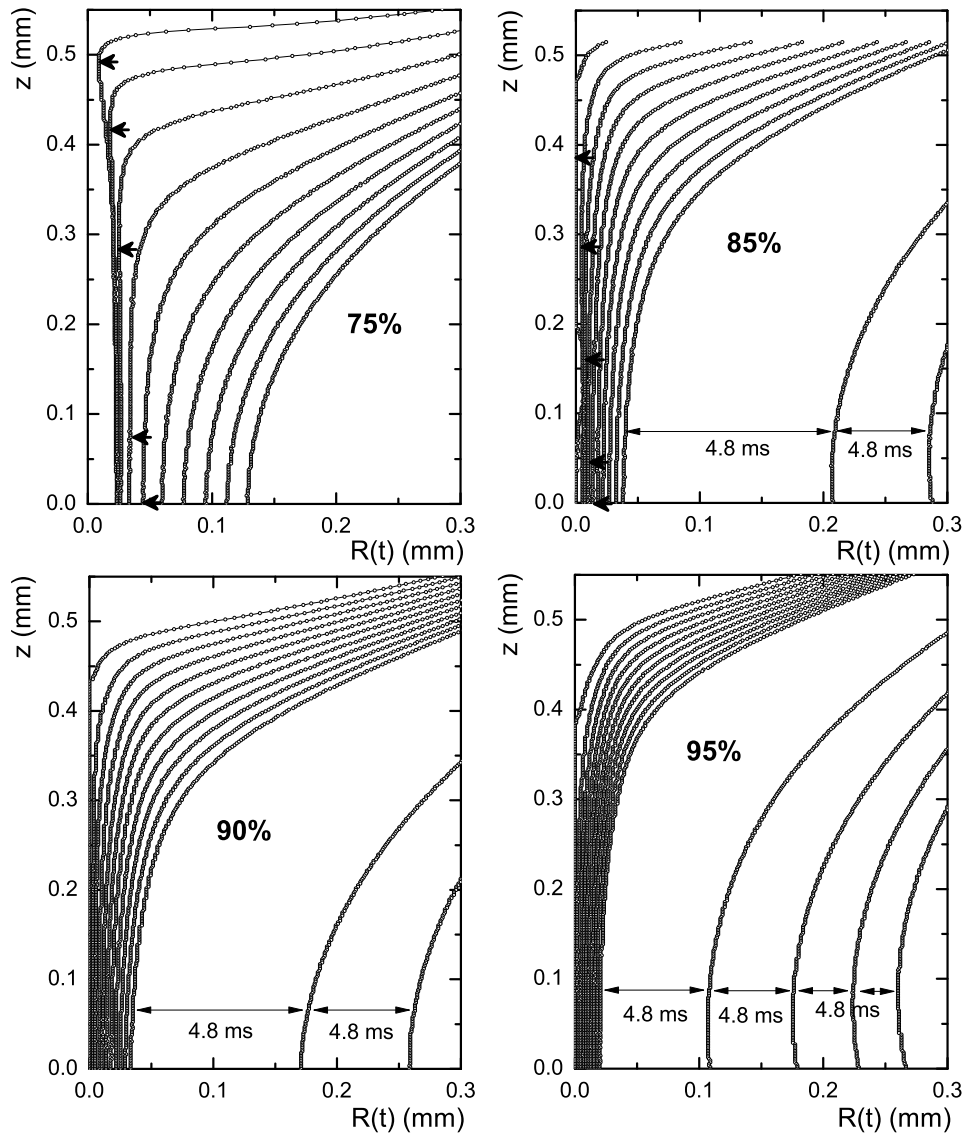


Figure 9: Time evolution of the filament profile  $R(z)$  for the glycerol/water mixtures of Fig. 6, at  $25^{\circ}\text{C}$ . The time intervals between the profiles are  $0.185\text{ ms}$ , larger time intervals are indicated in the graphs. Bold arrows indicate the position of the minimum radius  $R_{min}$  where this is not located at the mid-filament position  $z = 0$ .

325 is described by a power law as derived by [50, 37]

$$R_{min} = 0.64 \left( \frac{\gamma}{\rho} \right)^{\frac{1}{3}} (t_0 - t)^{\frac{2}{3}}, \quad (5)$$

326 is generally observed for low viscous fluids where the capillary pressure is  
 327 only resisted by the inertia of the accelerating fluid molecules.

328 The experimental data of the 85% solution in Fig. 5 are actually for a  
 329 similar glycerol concentration and viscosity as the numerical simulations by  
 330 Chen et al. [51] and the experiments of Rothert et al. [52] that predicted  
 331 and showed the existence of an IV thinning regime. The faster thinning data  
 332 in Fig. 5 prior to the onset of the linear regime are, however, caused by the  
 333 initially high axial curvature and lack of sufficient slenderness of the filament.  
 334 We can therefore not judge if the thinning prior to the onset of the IV regime  
 335 is following a V or PF scaling.

336 The general question, if the overall thinning dynamics of a filament are  
 337 controlled by viscosity (as for the 95% and 90% glycerol solutions in Figs. 5,  
 338 6 and 9) or by inertia (the 85% and 75% glycerol solutions) can be answered  
 339 by calculating the Ohnesorge number

$$Oh = \frac{\eta}{\sqrt{\rho\gamma R}}. \quad (6)$$

340 that compares the timescales of a viscosity controlled breakup  $t_v = \eta R/\gamma$   
 341 and an inertia controlled breakup  $t_\rho = 0.3413\sqrt{\rho R^3/\gamma}$  [37]. In order to  
 342 determine the critical value of the Ohnesorge number below which a filament  
 343 breakup will be controlled by inertia rather than the viscosity, one needs to  
 344 compare the actual velocities with which the filament thins in the PF and  
 345 in the V regime. Outgoing from eqs. (2) and (5) one can obtain via the

346 first derivatives the thinning velocities  $U = -dR/dt$  as  $U_\eta = 0.0709\gamma/\eta$  for  
 347 the viscous thinning regime and  $U_\rho = 0.3413\sqrt{\gamma/(\rho R)}$  for the potential flow  
 348 regime. Formulating then a Ohnesorge number via the ratio of these velocities  
 349 (rather than as a ratio of timescales as done in the derivation of Rodd et al.  
 350 [37]) we obtain the appropriate numerical front factor that describes the  
 351 correct transition value for the Ohnesorge number when  $U_\rho = U_\eta$ :

$$\frac{U_\rho}{U_\eta} = \frac{Oh}{0.2077}. \quad (7)$$

352 Using the initial radius of the cylindrical filament of  $R = 2$  mm we ob-  
 353 tain  $Oh = 1.09$  for the 95% glycerol solution and  $Oh = 0.08$  for the 75 %  
 354 solution ( $Oh$  values are also indicated in the figure 6). The Ohnesorge num-  
 355 ber of  $Oh = 0.21$  calculated for the solution of 85% that shows a breaking  
 356 behaviour right at the transition between viscous and inertia control is then  
 357 in excellent agreement with the the critical value of 0.2077 of eq. (7). Fur-  
 358 thermore, the experimental results in Fig. 6 are also in good agreement with  
 359 numerical calculations of the filament profiles for similar Ohnesorge numbers.  
 360 A comparison to Fig. 1d and 3b in [39] shows for example that the predicted  
 361 formation of the small bead on a string structure at  $Oh = 0.4$  and  $Oh = 0.2$   
 362 is actually observed in our experiments for the 75% solution at  $Oh = 0.21$ .

363 While the above classification via the Ohnesorge number allows a de-  
 364 termination of the ‘global’ or overall breaking behaviour, Eggers [49] has  
 365 shown that also during the thinning process any initially in the PF regime  
 366 starting filament will eventually turn over to an IV thinning. The minimum  
 367 filament radius at which this transition sets in can be determined from a  
 368 local Ohnesorge number [53, 51, 27, 26]. Assuming that this transition takes



369 place when the length scale that enters the Ohnesorge number (the radius  
 370  $R_{min}$ ) reaches a value so that the Ohnesorge number takes on the critical  
 371 value  $Oh^* = 0.2077$  of eq. (7), we can calculate the corresponding critical  
 372 minimum filament radius at which this transition sets in:

$$R^* = 23.2 \frac{\eta^2}{\rho\gamma}. \quad (8)$$

373 From a practical point of view the transition to the IV regime is done  
 374 at  $\sim 0.3Oh/0.2077$  [51] and the fully developed linear thinning regime can  
 375 therefore be observed at  $\sim 0.1R^*$ . For the 85% glycerol solution with a  
 376 viscosity of 77 mPa s this critical limit equates to  $0.1R^* = 0.8$  mm and the  
 377 linear IV thinning regime is therefore still within the observable limits in  
 378 Figure 5. However, for the 75% solution with a viscosity of 27 mPa s, this  
 379 transition radius calculates to  $R^* = 0.26$  mm and the clear onset of linear  
 380 IV thinning therefore to  $0.1R^* = 0.026$  mm. From these radii follows that  
 381 most of the thinning data observed in Figure 5 for the 75% solution is within  
 382 the transitional regime between PF and IV thinning, and the onset of linear  
 383 thinning is expected only at the last data point.

384 Since the viscosity enters eq. (8) squared, it becomes clear that for even  
 385 lower viscosities also the critical radius  $R^*$  will leave the observable window.  
 386 For aqueous systems with viscosities of 1 mPa s the critical radius  $R^*$  is of  
 387 order  $O(0.1\mu m)$  and the thinning dynamics in the observable diameter range  
 388 will follow solely a PF thinning and eq. (5). In the following section, that  
 389 focuses on the thinning dynamics of dilute aqueous polymer solutions, we  
 390 will therefore observe only the PF thinning dynamics before the onset of any  
 391 observable polymer contribution.

392 *3.2. Dilute Polymer Solutions*

393 In this section the filament thinning behaviour of a series of dilute aqueous  
394 solutions of polyethylene oxide with a molecular weight of 1.000.000 g/mol  
395 is investigated with the SRM. The solutions have a constant shear viscosity  
396 from 1 to 3 mPa s approximately, and will therefore show initially a thinning  
397 behaviour within the PF regime. For the capillary breakup experiments an  
398 initial aspect ratio of  $\Lambda_0 = 0.5$  and plate diameter  $D_p = 4$  mm were chosen  
399 as determined in the previous section for most reproducible results. In order  
400 to be able to observe short relaxation times in the inertial flow regime, a  
401 recording rate of 15000 frames per second was selected with a resolution of  
402 256 x 320 square pixel and 1.8  $\mu\text{m}/\text{pixel}$ .

403 In Figure 10 the evolution of the filament radius  $R_{min}$  with time is shown  
404 for the different PEO concentrations. For a better visualization the curves are  
405 shifted by a time  $t_p$  along the time axis so that the initial PF regimes collapse  
406 onto the pure solvent curve [4]. As it can be seen in Figure 10, the initial  
407 necking of all dilute polymer solutions is similar to the Newtonian solvent and  
408 following the PF thinning of eq. (5) (indicated by the solid line in Figure 10).  
409 The SRM assures that at the beginning of the thinning process the polymer  
410 molecules are unstretched and the capillary pressure is solely balanced by  
411 inertial acceleration in the fluid column. However, for high enough extension  
412 rates ( $\dot{\epsilon} \lambda > 0.5$ ) the chains will eventually undergo a coil-stretch transition,  
413 start to unravel and begin to balance with their resulting entropic stresses  
414 the squeezing action of surface tension. In this case close to  $t - t_p = 0$  a  
415 transition from the initial PF thinning regime to an elasto-capillary (EC)  
416 balance regime is observed and the necking fluid filament is formed into a

417 long thin thread that thins exponential with time. As indicated by the first  
 418 three pictures in Figure 10, the minimum filament radius is initially moving  
 419 towards the enddroplets as expected for a PF thinning. The thin filament  
 420 that forms (stabilized by the unraveling polymer) is therefore for the lower  
 421 polymer concentrations located on both sides between a large satellite drop in  
 422 the middle and the two enddrops [39, 40] (in the following we have evaluated  
 423 the evolution of the upper filament). Measurements of the thinning rate  
 424 in the elastic thinning regime can be used to estimate the relaxation time  
 425  $\lambda$  for the polymer solution in an extensional flow. As long as the finite  
 426 extensibility limit of the molecules is not yet reached the balance between  
 427 elastic stresses and capillary pressure results in an exponential decrease in  
 428 the filament radius, with a time constant corresponding to three times the  
 429 longest relaxation time of the fluid [29, 23, 54]

$$\frac{R_{min}}{R_0} = \left( \frac{GR_0}{2\gamma} \right)^{1/3} e^{\frac{-t}{3\lambda}}. \quad (9)$$

430 This exponential behaviour is clearly observed in the semi-log presenta-  
 431 tion of Figure 10 for the highest concentrated solution of 0.05%, indicated by  
 432 the straight fit line. Also for 0.02 and 0.01% this exponential decay is clearly  
 433 visible after an initial disturbance of an inertio elastic wave at the transition  
 434 from the PF to the EC thinning regime. The values for the respective re-  
 435 laxation times obtained from the fits of eq. (9) are given in Table 2. These  
 436 relaxation times determined with the slow retraction method are with 0.24  
 437 ms the lowest reliably reported so far for capillary thinning experiments, and  
 438 below the limit of 1 ms indicated by Rodd et al. [37].

439 The exponentially thinning filament in the EC regime develops prior to

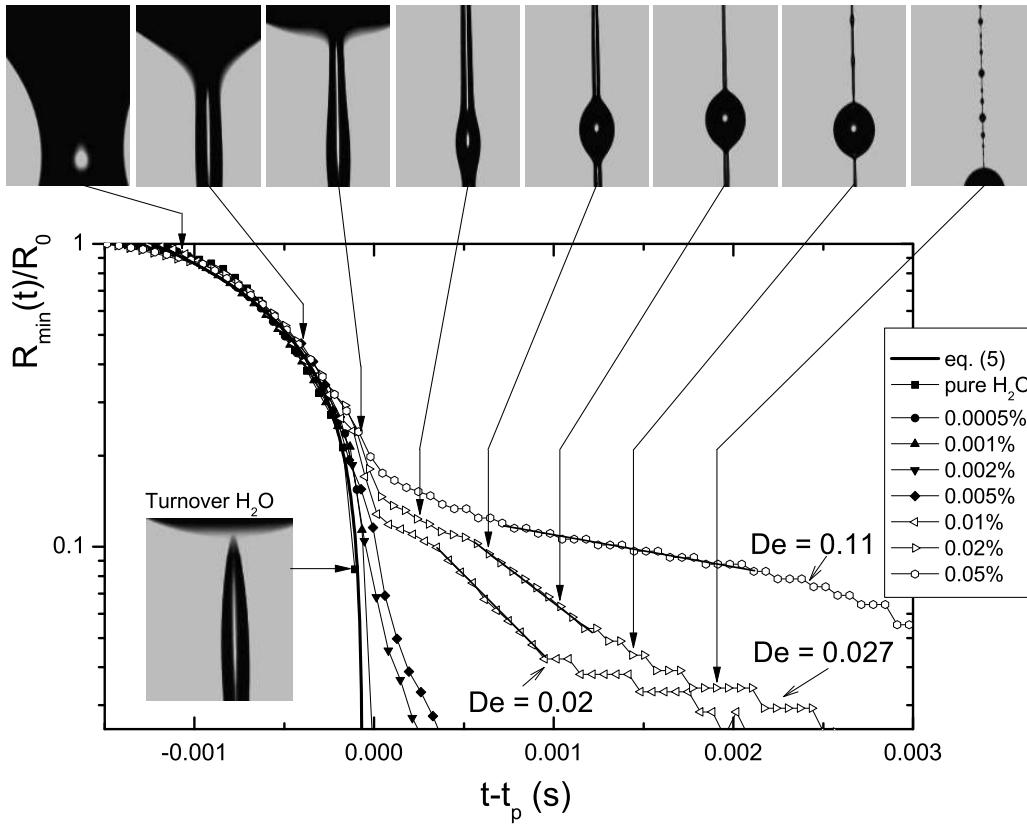


Figure 10: Time evolution of filament diameter for the different PEO concentrations, at  $25^{\circ}\text{C}$ . The straight lines on the three highest concentrations represent exponential fits following eq. (9).

440 breakup further instabilities that can be observed as the 'bead-on string'  
 441 structure in the last pictures of Figure 10 [54, 55]. Although the evaluation  
 442 of an exponential thinning regime is, in principle, also possible from the  
 443 string between the higher order generations of beads [56, 40], the induced  
 444 oscillations by the occurrence of the higher order satellites [40] induces too  
 445 much noise for a quantitative evaluation of the radius data and we restricted

Table 2: Relaxation times from capillary break-up experiments and Zimm relaxation times for the aqueous PEO solutions.

	$\lambda$ (ms)	$\lambda_Z$ (ms)
0.05%	1.38	0.107
0.02%	0.322	0.107
0.01%	0.240	0.107
0.005%	-	0.107
0.002%	-	0.107

446 the fit to obtain the relaxation time to the thinning regime before the onset  
 447 of the bead-on-string structure.

448 The experimentally observed diameter evolutions in Figure 10 are very  
 449 similar to the predictions of numerical simulations of [39] for low viscous  
 450 and weakly elastic polymer solutions. Calculating the respective Deborah  
 451 numbers  $De = \lambda/\sqrt{\rho R^3/\gamma}$  from the accessible relaxation times  $\lambda$  in Table 2  
 452 and the initial radius of  $R = 2$  mm (indicated in Figure 10), we can compare  
 453 the experimentally observed breaking behaviour in Fig. 10 to the simulations  
 454 in Fig. 3a of [39]. It is obvious that for both a Deborah number of  $De = 0.02$   
 455 as well as  $De = 0.1$  the experiments confirm the radius evolution predicted  
 456 by the simulations, in particular the figure sequence in Figure 10 for  $De =$   
 457  $0.027$  reflects the simulated profiles of Fig. 3b(Bottom) in [39] for  $De = 0.02$ .

### 458 3.3. Lower concentration limit for the determination of a relaxation time

459 One could also be tempted to perform an exponential fit on the thinning  
 460 data of the lower concentrations of 0.005 % and 0.002%. However, the ca-  
 461 pability of a capillary breakup experiment to extract a relaxation time from

462 the thinning data is limited to a critical minimum concentration. As laid out  
 463 by Clasen et al. [5], for higher viscosity solutions a lower limit of the visi-  
 464 ble effects of the polymer concentration on the thinning dynamics is reached  
 465 when even the fully unraveled polymer chains will carry less stress than the  
 466 solvent. This can be related to the lower viscosity solutions in this paper  
 467 when looking again at the Ohnesorge number of eq. (6). The viscosity  $\eta$   
 468 that enters the Ohnesorge number for a dilute polymer solution consists of  
 469 a contribution of the solvent and of the polymer  $\eta = \eta_s + \eta_p$ . For a low  
 470 viscous solvent in an extensional flow the solvent contribution  $\eta_s$  is negligible  
 471 and the viscosity originates primarily from the viscosity contribution  $\eta_p$  of  
 472 the unraveling polymer chains. Following a FENE model description of the  
 473 polymer stress in a dilute solution in an uniaxial flow, the stress originating  
 474 from the polymer coils can be described as  $GA_{zz}$ , where

$$G = nkT = \frac{cN_A k_B T}{M_w} \quad (10)$$

475 is the modulus of the polymer in solution (with  $N_A$  and  $k_B$  as the Avo-  
 476 gadro and Boltzman constants respectively), and  $A_{zz}$  is the axial component  
 477 of the conformation tensor  $\mathbf{A}$  (defined as the ensemble average second mo-  
 478 ment configuration tensor of the entire chain,  $\mathbf{A} = \frac{\langle \mathbf{Q}\mathbf{Q} \rangle}{Q_{eq}^2/3}$ , normalized with  
 479 the equilibrium coil end-to-end distance  $Q_{eq}$ ). The polymer contribution to  
 480 the extensional viscosity  $\eta_p = GA_{zz}/\dot{\epsilon}$  reaches its maximum when the poly-  
 481 mer chains approach their finite extensibility limit where  $A_{zz} \sim L^2$  and the  
 482 extensional viscosity reduces to the constant value  $2G\lambda L^2$  [5] (here  $L^2$  de-  
 483 notes in FENE terminology the finite extensibility limit of the polymer coils  
 484 that is defined as the trace of the conformation tensor of the polymer coil,

485  $tr\mathbf{A}$ , at full stretch). With these assumptions the local Ohnesorge number  
 486 reduces at the finite extensibility limit to [57]

$$Oh = \frac{2G\lambda L^2}{3\sqrt{\rho\gamma R}}. \quad (11)$$

487 For a given modulus  $G$  (or concentration  $c$  via eq. (10)) this equation can  
 488 be solved for a critical radius  $R_{Oh}$  at which the initial PF thinning changes to  
 489 a V thinning regime controlled by the constant viscosity of the fully unraveled  
 490 polymer chains:

$$R_{Oh} = 23.18 \frac{(\frac{2}{3}G\lambda L^2)^2}{\rho\gamma}. \quad (12)$$

491 The numerical front factor arises from the critical value for the Ohnesorge  
 492 number  $Oh = 0.2077$  from eq. (7). This radius  $R_{Oh}$  at which this transition  
 493 from the PF to the V regime is observed decreases with decreasing polymer  
 494 concentration and eventually leaves the observation window.

495 However, the above assumption of fully unraveled polymer coils can lead  
 496 to an overestimation of this critical radius, since the polymer coils first have  
 497 to unravel during the thinning process in order to reach the finite extensibility  
 498 limit. The onset of unraveling will not occur at the initial filament radius  
 499  $R_0$ , but only when the extension rate  $\dot{\epsilon} = -(2/R)(dR/dt)$  in the thinning  
 500 filament overcomes the critical limit  $\dot{\epsilon}\lambda = 0.5$  that marks the coil-stretch  
 501 transition of a polymer. Using the extension rate  $\dot{\epsilon}_\rho$  for an inertia controlled  
 502 filament thinning (retaining the numerical factor of eq. (5) obtained from  
 503 the similarity solutions for inertio-capillary breakup [37])

$$\dot{\epsilon}_\rho = 0.68 \sqrt{\frac{\gamma}{\rho R^3}} \quad (13)$$

504 we can solve for the critical filament radius  $R_{0,c}$  at which the coil-stretch  
 505 transition will begin

$$R_{0,c} = 1.23 \left( \frac{\gamma \lambda^2}{\rho} \right)^{\frac{1}{3}}. \quad (14)$$

506 Assuming an affine deformation of the unraveling polymer chain with  
 507 the fast elongating filament, the axial component of the conformation ten-  
 508 sor  $\mathbf{A}$  evolves with the radius as  $A_{zz}R^4 = A_{zz,0}R_{0,c}^4$  [58] (The assumption  
 509 of an affine polymer deformation is justified by recognizing that at  $R_{0,c}$  a  
 510 local intrinsic Deborah number that compares the inertia controlled time  
 511 to break  $t_\rho$  with the relaxation time  $\lambda$  of the polymer [27] calculates to  
 512  $De_0 = t_\rho/\lambda = (\gamma\lambda^2/(\rho R_{0,c}))^{0.5} = 0.73$ . So for any instant happening at  
 513  $t < t_\rho(R_{0,c})$  (e.g. the transition to an EC balance, or the polymers reach-  
 514 ing their finite extensibility) the polymer relaxation can be neglected). An  
 515 advantage of the SRM in order to create the thinning filament is now that  
 516 the polymer coil will be initially in a relaxed state and therefore  $A_{zz,0} = 1$   
 517 at  $R = R_{0,c}$ . In this case we can relate the filament radius  $R$  to the state of  
 518 deformation of the polymer  $A_{zz}$  via

$$R = \frac{R_{0,c}}{A_{zz}^{\frac{1}{4}}} \quad (15)$$

519 The radius  $R_{L^2}$ , at which the polymer coils approach their finite extensi-  
 520 bility limit so that one can assume  $A_{zz} \sim L^2$  is then

$$R_{L^2} = \frac{R_{0,c}}{L^{\frac{1}{2}}}. \quad (16)$$

521 Only if the radius  $R_{Oh}$  (eq. (12)) at which the critical Ohnesorge number  
 522 is reached is below this critical filament radius  $R_{L^2}$  we will observe a transition



523 from the PF to a V regime controlled by the viscosity  $2G\lambda L^2$  of the already  
 524 fully extended chains.

525 If the stresses that originate from the unraveling polymer coils become  
 526 sufficiently large to balance the surface pressure before  $R_{L^2}$  is reached, we will  
 527 observe a transition from the initial PF regime to an elasto-capillary (EC)  
 528 balance during which the polymer chains are still further unraveling and have  
 529 not reached their finite extensibility limit yet. Only in this EC regime is it  
 530 possible to obtain via eq. (9) a relaxation time  $\lambda$  from the thinning dynamics.

531 However, the polymer concentration needs to be sufficiently high in order  
 532 create enough polymers stress to stabilize an EC balance before the finite  
 533 extensibility limit at  $R_{min}$  is reached. Similar to [5] a critical minimum  
 534 polymer concentration  $c_{min}$  can be defined at the point where at least half  
 535 the surface pressure is balanced by the stresses originating from the stretching  
 536 polymers. With the polymer stress equal to  $GA_{zz}$  this condition is met when

$$\frac{\gamma}{R} = 2GA_{zz} \quad (17)$$

537 Combining this criterion with eq. (15) gives then the relation between a  
 538 modulus (or concentration) and a critical radius  $R_{EC}$  at which the polymer  
 539 stresses start to dominate the thinning dynamics and would show a transition  
 540 to an elasto-capillary balance

$$R_{EC} = R_{0,c} \left( \frac{2GR_{0,c}}{\gamma} \right)^{\frac{1}{3}} \quad (18)$$

541 Setting the critical radii  $R_{L^2}$  and  $R_{EC}$  of eqs. (16) and (18) equal gives  
 542 then the lower limit for the modulus  $G_{low}$  at which an observable onset of a  
 543 polymer contribution to the thinning dynamics coincides with the polymer

544 just having reached its finite extensibility limit

$$G_{low} = \frac{\gamma}{2L^{\frac{3}{2}}R_{0,c}}. \quad (19)$$

545 The observation of an exponential thinning regime required for the de-  
546 termination of a relaxation time with eq. (9) from a Caber experiment is  
547 therefore not possible for a modulus below  $G_{low}$  or a concentration below the  
548 related critical concentration  $c_{low}$ . This critical concentration limit is larger  
549 than the minimum concentration  $c_{min}$  derived in [5]. While  $c_{min}$  in [5] gives  
550 the critical concentration below which the polymer will not affect the thin-  
551 ning dynamics and delay the breaking process,  $c_{low}$  indicates the (higher)  
552 concentration where the polymer will not only delay the breaking process,  
553 but where also the finite extensibility limit is not yet approached and a true  
554 exponential thinning regime following eq. (9) can be observed.

555 Still, the lower limit of the modulus  $G_{low}$  is just an order of magnitude  
556 estimation for two reasons. First of all, the relaxation time  $\lambda$  that enters  
557 eq. (19) via the critical radius  $R_{0,c}$  (eq. (14)) is not known *a priori*. An  
558 estimate of  $\lambda$  for dilute solutions with the Zimm relaxation time  $\lambda_Z$  (eq. 21)  
559 (as done below) is going to underestimate  $\lambda$ . Even the lowest relaxation times  
560 in Table 2 that could be reliably determined from the exponential thinning  
561 profile in the capillary breakup experiments of Fig. 10 are roughly an order  
562 of magnitude larger than the Zimm relaxation time  $\lambda_Z$ . Using the Zimm  
563 time as an estimate in eq. (14) will therefore lead to an overestimation of  
564  $G_{low}$  by a factor of  $\sim 5$ . Secondly, the stretching polymer chains will leave  
565 their linear response regime much earlier than at their finite extensibility  
566 limit. In [58] a linear response regime was estimated to hold until polymer

567 stretches of  $A_{zz} = 0.1L^2$ . Neglecting this criterion when calculating  $G_{low}$   
568 leads therefore to an underestimation by a factor of  $\sim 5$ . Since both these  
569 effects work in opposite direction and by roughly the same factor, eq. (19)  
570 gives still a good order of magnitude estimation of the lower limit of the  
571 modulus. This can readily be seen when calculating the absolute lower limit  
572 for the concentration,  $c_{low}$ , by combining eqs. (10), (14) and (19)

$$c_{low} = \frac{1}{2.46} \frac{M_w}{N_A k_B T} \left( \frac{\gamma^2 \rho}{\lambda^2} \right)^{\frac{1}{3}} \frac{1}{L^{\frac{3}{2}}}. \quad (20)$$

573 An estimate for the relaxation time  $\lambda$  can be done with the Zimm time  
574  $\lambda_Z$  [5]

$$\lambda_Z = \frac{1}{U_{\eta\tau}} \frac{[\eta] \eta_s M_w}{N_A k_B T}. \quad (21)$$

575 The universal ratio  $U_{\eta\tau}$  [59] can be estimated from the excluded volume  
576 exponent  $\nu$  as described by [4] via  $U_{\eta\tau} = \zeta(3\nu)$  with  $\zeta$  as the Riemann zeta  
577 function. For  $\nu = 0.55$  for PEO in aqueous solution [4]  $U_{\eta\tau}$  calculates to  
578 0.463. The intrinsic viscosity  $[\eta]$  can be calculated from the appropriate  
579 Mark-Houwink-Sakurada equation which is tabulated for the present system  
580 in [60] as  $[\eta] = 0.072 M_w^{3\nu-1}$ . With this we obtain for the Zimm relaxation  
581 time  $\lambda_Z = 0.107$  ms. The finite extensibility parameter  $L^2$  can be obtained  
582 from molecular parameters as the CC bond angle  $\theta$ , the number of bonds  $j$   
583 in a monomer unit with molar mass  $M_u$  and the characteristic ratio  $C_\infty$  for  
584 a given polymer [5]

$$L^2 = \frac{3}{k_\alpha^2} \left[ \frac{j \sin^2(\theta/2) M_w}{C_\infty M_u} \right]^{2(1-\nu)}. \quad (22)$$

585  $C_\infty$  is reported in [60] as 4.8 for  $j = 3$  and an averaged bond angle  $\theta$   
 586 in the PEO monomer unit taken as the CC bond angle. The additionally  
 587 introduced swelling ratio  $k_\alpha^2$  that takes into account the polymer coil expan-  
 588 sion in the relatively good solvent can be estimated by from the excluded  
 589 volume exponent  $k_\alpha^2 \approx \zeta(3\nu)/\zeta(1.5)$  [61] and equates for the current system  
 590 to  $k_\alpha^2 = 0.829$ . With this the finite extensibility parameter calculates to  
 591  $L^2 = 13713$  and we can now obtain the lower limit for the concentration  
 592 from eq. (20) as  $c_{low} = 0.009\%$ .

593 This calculated value is in good agreement with the experimental data in  
 594 Figure 10. For a concentration of  $c = 0.01\%$  and all higher concentrations  
 595 (open symbols) that are above the calculated critical value  $c_{low}$  a sufficiently  
 596 long exponential thinning regime is clearly detectable. For the next smaller  
 597 concentration of  $c = 0.005\%$  (indicated by filled symbols) that is already  
 598 below the calculated lower limit we can still observe an influence of the poly-  
 599 mer on the breaking behaviour and a delayed breaking in comparison to the  
 600 pure solvent. However, a clear exponential thinning regime is not observed.  
 601 It might be tempting to do an exponential fit to the thinning data for the  
 602 concentration  $c = 0.005\%$  (and also for  $c = 0.002\%$ ) that still show a de-  
 603 layed breakup time, in order to extract a relaxation time. However, outgoing  
 604 from our analysis the thinning data will already be in the finite extensibility  
 605 limit of the polymer and the apparent relaxation time will be shorter than  
 606 the actual one. We attribute in the literature reported experimental relax-  
 607 ation times below the Zimm time to attempts to fit the thinning data of  
 608 concentrations below the critical limit  $c_{low}$ .

609 For the lowest experimental polymer concentrations of  $c = 0.001\%$  and

610  $c = 0.0005\%$  a calculation of the radius  $R_{EC}$  from eq. (18) at which an onset  
 611 of a delayed thinning caused by the polymer can be expected yields values  
 612 that are below the observable window in Fig. 10. And indeed, we do not  
 613 observe a deviation from the thinning dynamics of the pure solvent in Fig.  
 614 10 for  $c = 0.001\%$  and  $c = 0.0005\%$ . Furthermore, for these dilutions as well  
 615 as for the pure solvent the minimum filament diameter is eventually located  
 616 within an indentation of the terminal drop, so that the 2-dimensional projection  
 617 of the filament profile does not allow to observe the thinning dynamics beyond  
 618 this so called 'turnover' point (indicated in Figure 10 for the case of pure  
 619 water).

#### 620 4. Conclusions

621 Conducting a capillary breakup experiment with the initial liquid bridge  
 622 close to the critical aspect ratio  $\Lambda_{S,break}$  of a statically stable state enables one  
 623 to quantitatively investigate the thinning dynamics of low viscosity liquids.  
 624 Using a slow retraction of the endplates that confine the liquid bridge in  
 625 order to overcome the critical value of  $\Lambda_{S,break}$  induces an axially symmetric  
 626 thinning and minimizes effects of inertia induced oscillations of the end drops  
 627 and the connecting filament. This slow retraction method allowed to follow  
 628 the thinning dynamics of a series of Newtonian glycerol in water solutions  
 629 with viscosities that span a range of 350 - 27 mPa s. The transition between  
 630 a viscosity and an inertia controlled thinning, in particular the radius of the  
 631 filament at which this transition takes place can be obtained from a local  
 632 Ohnesorge number  $Oh$  (eq. (6)) that uses the radius  $R_{min}(t)$  as the critical  
 633 length scale. The numerical value for  $Oh$  at the transition could be obtained

634 from a balance of the thinning velocities in the viscous (V) flow regime and  
 635 the inertial (PF) flow regime to  $Oh = 0.2077$ . Equating the the critical radius  
 636 of the transition from this local Ohnesorge number shows that the onset of the  
 637 V regime shifts with decreasing viscosity to lower filament radii in accordance  
 638 with the experimental observations for the glycerol solutions. The thinning  
 639 dynamics allow for a clear observation of a V thinning regime for viscosities of  
 640 320 and 150 mPa s and a IV thinning for 77 mPa s. However, the SRM leads  
 641 for Newtonian liquids to a high axial curvatures of the thinning filament,  
 642 so that an evaluation of the thinning data with the similarity solutions of  
 643 eqs. (2) and (4) is only possible for small radii where the mean curvature  
 644  $\kappa = 1/R_{min} - 1/R_z$  approaches the radial curvature  $1/R_{min}$ . A practical  
 645 value for the general 'slenderness' requirement for the application of similarity  
 646 solution and the range of radii where linear fits of  $R_{min} \sim (t_0 - t)$  can be  
 647 used to extract material properties from capillary thinning experiments has  
 648 shown to be  $\kappa R_{min} = 1.006$ .

649 For dilute polymer solutions with a shear viscosity of  $O(1 \text{ mPa s})$  the  
 650 initial thinning dynamics of a liquid bridge (for which the endplate separa-  
 651 tion crosses the critical aspect ratio  $\Lambda_{S,break}$ ) follow the PF thinning law  
 652 of eq. (5). However, as soon as the unraveling polymer chains carry more  
 653 stress than the surrounding solvent, the thinning dynamics switch over to an  
 654 EC type thinning and allow to extract a relaxation time via eq. (9). Due  
 655 to the initial PF thinning with local minimum radii close to the enddrops  
 656 one observes two cylindrical filaments stabilized by the EC balance, with a  
 657 large satellite drop in the middle. The observability of an EC thinning of the  
 658 cylindrical filaments is limited by a critical concentration  $c_{low}$  of the poly-

659 mer. If the unraveling polymer chains reach their finite extensibility limit  
660 (at a concentration independent filament radius  $R_{L2}$  (eq. (16))) *before* the  
661 polymer stress becomes sufficiently large to balance the capillary pressure  
662 (at a concentration dependent filament radius  $R_{EC}$  (eq. (18))) the EC bal-  
663 ance will not be observable. Setting  $R_{L2}$  and  $R_{EC}$  equal allows therefore to  
664 determine a lower limit for the modulus,  $G_{low}$  (eq. (19)) (or concentration  
665  $c_{low}$ ), below which a capillary breakup experiment will not allow the extrac-  
666 tion of the relaxation time. Accounting for this concentration limit (which  
667 could be calculated for the investigated solutions of polystyrene in DEP to  
668  $c_{low} = 0.009\%$ ) a reliable relaxation time in extension as low as  $240\ \mu\text{s}$  at a  
669 concentration of  $0.01\%$  PEO could be determined with the SRM.

## 670 **Acknowledgments**

671 The authors would like to acknowledge financial support from the ERC  
672 starting grant 203043 NANOFIB.

## 673 **References**

- 674 [1] V. M. Entov, A. L. Yarin, Influence of elastic stresses on the capillary  
675 breakup of jets of dilute polymer solutions, *Fluid Dynamics* 19 (1984)  
676 21–29.
- 677 [2] A. V. Bazilevsky, V. M. Entov, A. N. Rozhkov, Breakup of an Ol-  
678 droyd liquid bridge as a method for testing the rheological properties of  
679 polymer solutions, *Polymer Science* 43 (2001) 716.

- 680 [3] M. Stelter, G. Brenn, A. L. Yarin, R. P. Singh, F. Durst, Investigation of  
681 the elongation behavior of polymer solutions by means of an elongational  
682 rheometer, *Journal of Rheology* 46 (2002) 507.
- 683 [4] V. Tirtaatmadja, G. H. McKinley, J. J. Cooper-White, Drop formation  
684 and breakup of low viscosity elastic fluids: Effects of molecular weight  
685 and concentration, *Physics of Fluids* 18 (2006) 043101.
- 686 [5] C. Clasen, J. P. Plog, W. M. Kulicke, M. Owens, C. Macosko, L. E.  
687 Scriven, M. Verani, G. H. McKinley, How dilute are dilute solutions in  
688 extensional flows?, *Journal of Rheology* 50 (2006) 849–881.
- 689 [6] S. Middleman, Stability of a viscoelastic jet, *Chemical Engineering*  
690 *Science* 20 (1965) 1037–1040.
- 691 [7] M. Goldin, J. Yerushalmi, R. Pfeffer, R. Shinnar, Breakup of a laminar  
692 capillary jet of a viscoelastic fluid, *Journal of Fluid Mechanics* 38 (1969)  
693 689–711.
- 694 [8] D. W. Bousfield, R. Keunings, G. Marrucci, M. M. Denn, Nonlinear  
695 analysis of the surface tension driven breakup of viscoelastic filaments,  
696 *Journal of Fluid Mechanics* 21 (1986) 79–97.
- 697 [9] Y. Christanti, L. M. Walker, Surface tension driven jet break up of  
698 strain-hardening polymer solutions, *Journal of Non-Newtonian Fluid*  
699 *Mechanics* 100 (2001) 9–26.
- 700 [10] Y. Amarouchene, D. Bonn, J. Meunier, H. Kellay, Inhibition of the  
701 finite-time singularity during drop fission of a polymeric fluid, *Physical*  
702 *Review Letters* 86 (2001) 3558.



- 703 [11] R. Sattler, C. Wagner, J. Eggers, Blistering pattern and formation of  
704 nanofibers in capillary thinning of polymer solutions, *Physical Review*  
705 *Letters* 100 (2008) 164502.
- 706 [12] J. Meissner, Development of an uniaxial extensional rheometer for uni-  
707 axial extension of polymer melts, *Transactions of the Society of Rheol-*  
708 *ogy* 16 (1972) 405.
- 709 [13] J. Meissner, J. Hostettler, A new elongational rheometer for polymer  
710 melts and other highly viscoelastic liquids, *Rheologica Acta* 33 (1994)  
711 1–21.
- 712 [14] H. Münstedt, New universal extensional rheometer for polymer melts -  
713 measurements on a polystyrene sample, *Journal of Rheology* 23 (1979)  
714 421–436.
- 715 [15] H. Münstedt, S. Kurzbeck, L. Egersdörfer, Influence of molecular struc-  
716 ture on rheological properties of polyethylenes. ii. elongational behavior,  
717 *Rheologica Acta* 37 (1998) 21–29.
- 718 [16] R. Haas, W. M. Kulicke, Flow behavior of dilute polyacrylamide solu-  
719 tions through porous-media. 2. Indirect determination of extremely high  
720 molecular-weights and some aspects of viscosity decrease over long-time  
721 intervals, *Industrial and Engineering Chemistry Fundamentals* 23 (1984)  
722 316–319.
- 723 [17] G. G. Fuller, C. A. Cathey, B. Hubbard, B. E. Zebrowski, Extensional  
724 viscosity measurements for low-viscosity fluids, *Journal of Rheology* 31  
725 (1987) 235–249.

- 726 [18] G. M. Harrison, J. Remmelgas, L. G. Leal, Comparison of dumbbell-based  
727 theory and experiment for a dilute polymer solution in a corotating two-  
728 roll mill, *Journal of Rheology* 43 (1999) 197–218.
- 729 [19] S. L. Anna, G. McKinley, D. A. Nguyen, T. Sridhar, S. J. Muller,  
730 J. Huang, D. F. James, An interlaboratory comparison of measurements  
731 from filament-stretching rheometers using common test fluids, *Journal*  
732 *of Rheology* 45 (2001) 83–114.
- 733 [20] T. Sridhar, V. Tirtaatmadja, D. A. Nguyen, R. K. Gupta, Measurement  
734 of extensional viscosity of polymer-solutions, *Journal of Non-Newtonian*  
735 *Fluid Mechanics* 40 (1991) 271–280.
- 736 [21] G. H. McKinley, T. Sridhar, Filament-stretching rheometry of complex  
737 fluids, *Annual Review of Fluids Mechanics* 34 (2002) 375–415.
- 738 [22] A. V. Bazilevsky, V. M. Entov, A. N. Rozhkov, Liquid filament mi-  
739 crorheometer and some of its applications, *Third European Rheology*  
740 *Conference*, D.R. Oliver (ed.), Elsevier Applied Science., 1990.
- 741 [23] S. L. Anna, G. H. McKinley, Elasto Capillary Thinning and Breakup of  
742 Model Elastic Liquids, *Journal of Rheology* 45 (2001) 115–138.
- 743 [24] G. H. McKinley, A. Tripathi, How to extract the Newtonian viscosity  
744 from capillary breakup measurements in a filament rheometer, *Journal*  
745 *of Rheology* 44 (2000) 653–671.
- 746 [25] P. Doshi, R. Suryo, O. E. Yildirim, G. H. McKinley, O. A. Basaran,  
747 Scaling in pinch-off of generalized Newtonian fluids, *Journal of Non-*  
748 *Newtonian Fluid Mechanics* 113 (2003) 1–27.

- 749 [26] R. Suryo, O. A. Basaran, Local dynamics during pinch-off of liquid  
750 threads of power law fluids: Scaling analysis and self-similarity, *Journal*  
751 *of Non-Newtonian Fluid Mechanics* 138 (2006) 134–160.
- 752 [27] G. H. McKinley, Visco-elasto-capillary thinning and break-up of com-  
753 plex fluids, *Rheology Reviews* (2005) 1–48.
- 754 [28] K. Niedzwiedz, O. Arnolds, N. Willenbacher, R. Brummer, How to char-  
755 acterize yield stress fluids with capillary breakup extensional rheometry  
756 (caber)?, *Applied Rheology* 19 (2009) 10.
- 757 [29] V. M. Entov, E. J. Hinch, Effect of a spectrum of relaxation times on  
758 the capillary thinning of a filament of elastic fluids, *Journal of Non-*  
759 *Newtonian Fluid Mechanics* 72 (1997) 31–54.
- 760 [30] R. F. Liang, M. R. Mackley, Rheological characterization of the time  
761 and strain dependence for polyisobutylene solutions, *Journal of Non-*  
762 *Newtonian Fluid Mechanics* 52 (1994) 387–405.
- 763 [31] A. V. Bazilevskii, V. M. Entov, M. M. Lerner, A. N. Rozhkov, Degrada-  
764 tion of polymer solution filaments, *Vysokomolekulyarnye Soedineniya*  
765 *Seriya A and Seriya B* 39 (1997) 474–482.
- 766 [32] M. Stelter, G. Brenn, Validation and application of a novel elongational  
767 device for polymer solutions, *Journal of Rheology* 44 (2000) 595–616.
- 768 [33] J. P. Plog, W. M. Kulicke, C. Clasen, Influence of the molar mass distri-  
769 bution on the elongational behaviour of polymer solutions in capillary  
770 breakup, *Applied Rheology* 15 (2005) 28–37.

- 771 [34] B. Yesilata, C. Clasen, G. H. McKinley, Nonlinear shear and exten-  
772 sional flow dynamics of wormlike surfactant solutions, *Journal of Non-*  
773 *Newtonian Fluid Mechanics* 133 (2006) 73–90.
- 774 [35] E. Miller, C. Clasen, J. P. Rothstein, The effect of step-stretch param-  
775 eters on capillary breakup extensional rheology (caber) measurements,  
776 *Rheologica Acta* 48 (2009) 625–639.
- 777 [36] C. Clasen, Capillary breakup extensional rheometry of semi-dilute poly-  
778 mer solutions, *Korea-Australia Rheology Journal* (2010) accepted.
- 779 [37] L. E. Rodd, T. P. Scott, J. J. Cooper-White, G. H. McKinley, Capillary  
780 break-up rheometry of low-viscosity elastic fluids, *Applied Rheology* 15  
781 (2005) 12–27.
- 782 [38] D. C. Vadillo, T. R. Tuladhar, A. C. Mulji, S. Jung, S. D. Hoath, M. R.  
783 Mackley, Evaluation of the inkjet fluid’s performance using the ”cam-  
784 bridge trimaster” filament stretch and break-up device, *Journal of Rhe-*  
785 *ology* 54 (2010) 261–282.
- 786 [39] P. P. Bhat, S. Appathurai, M. T. Harris, M. Pasquali, G. H. McKinley,  
787 O. A. Basaran, Formation of beads-on-a-string structures during break-  
788 up of viscoelastic filaments, *Nature Physics* 6 (2010) 625–631.
- 789 [40] A. M. Ardekani, V. Sharma, G. H. McKinley, Dynamics of bead forma-  
790 tion, filament thinning and breakup in weakly viscoelastic jets, *Journal*  
791 *of Fluid Mechanics* accepted (2010).
- 792 [41] N. F. Morrison, O. G. Harlen, Viscoelasticity in inkjet printing, *Rheo-*  
793 *logica Acta* 49 (2010) 619–632.

- 794 [42] S. D. Hoath, I. M. Hutchings, G. D. Martin, T. R. Tuladhar, M. R.  
795 Mackley, D. Vadhilo, Links between ink rheology, drop-on-demand jet  
796 formation, and printability, *Journal of Imaging Science and Technology*  
797 53 (2009) 8.
- 798 [43] B. J. de Gans, P. C. Duineveld, U. S. Schubert, Inkjet printing of  
799 polymers: State of the art and future developments, *Advanced Materials*  
800 16 (2004) 203–213.
- 801 [44] L. A. Slobozhanin, J. M. Perales, Stability of liquid bridges between  
802 equal disks in an axial gravity-field, *Physics of Fluids A-Fluid Dynamics*  
803 5 (1993) 1305–1314.
- 804 [45] M. P. Brenner, J. R. Lister, H. A. Stone, Pinching threads, singularities  
805 and the number 0.0304..., *Physics of Fluids* 8 (1996) 2827–2836.
- 806 [46] D. T. Papageorgiou, On the breakup of viscous-liquid threads, *Physics*  
807 *of Fluids* 7 (1995) 1529–1544.
- 808 [47] G. H. McKinley, A. Tripathi, How to extract the Newtonian viscosity  
809 from capillary breakup measurements in a filament rheometer, *Journal*  
810 *of Rheology* 44 (2000) 653–670.
- 811 [48] S. H. Spiegelberg, D. C. Ables, G. H. McKinley, The role of end-effects  
812 on measurements of extensional viscosity in filament stretching rheome-  
813 ters, *Journal of Non-Newtonian Fluid Mechanics* 64 (1996) 229–267.
- 814 [49] J. Eggers, Nonlinear dynamics and breakup of free-surface flows, *Re-*  
815 *views of Modern Physics* 69 (1997) 865–929.

- 816 [50] R. F. Day, E. J. Hinch, J. R. Lister, Self-similar capillary pinchoff of an  
817 inviscid fluid, *Physical Review Letters* 80 (1998) 704–707.
- 818 [51] A. U. Chen, P. K. Notz, O. A. Basaran, Computational and experimen-  
819 tal analysis of pinch-off and scaling, *Physical Review Letters* 88 (2002)  
820 174501.
- 821 [52] A. Rothert, R. Richter, I. Rehberg, Transition from symmetric to asym-  
822 metric scaling function before drop pinch-off, *Physical Review Letters*  
823 87 (2001) 084501.
- 824 [53] T. A. Kowalewski, On the separation of droplets from a liquid jet, *Fluid*  
825 *Dynamics Research* 17 (1996) 121–145.
- 826 [54] C. Clasen, J. Eggers, J. L. Fontelos, G. H. McKinley, The beads-on-  
827 string structure of viscoelastic threads, *Journal of Fluid Mechanics* 556  
828 (2006) 283–308.
- 829 [55] J. Li, M. A. Fontelos, Drop dynamics on the beads-on-string structure  
830 for viscoelastic jets: A numerical study, *Physics of Fluids* 15 (2003) 922.
- 831 [56] M. S. N. Oliveira, R. Yeh, G. H. McKinley, Iterated stretching, exten-  
832 sional rheology and formation of beads-on-a-string structures in polymer  
833 solutions, *Journal of Non-Newtonian Fluid Mechanics* 137 (2006) 137–  
834 148.
- 835 [57] O. G. Harlen, Jet break-up of polymer solutions in inkjet printing, in:  
836 <http://www.ima.umn.edu/2009-2010/W10.12-16.09/>.

- 837 [58] C. Clasen, J. Bico, V. M. Entov, G. H. McKinley, 'Gobbling drops':  
838 the jetting-dripping transition in flows of polymer solutions, *Journal of*  
839 *Fluid Mechanics* 636 (2009) 5–40.
- 840 [59] H. C. Oettinger, *Stochastic Processes in Polymeric Liquids*, Springer  
841 Verlag, Berlin, 1996.
- 842 [60] J. Brandrup, E. H. Immergut, *Polymer Handbook*, John Wiley & Sons,  
843 New York, 4th edition, 1999.
- 844 [61] G. H. McKinley, personal communication, 2002.